Effect of the Core/Shell Latex Particle Interphase on the Mechanical Behavior of Rubber-Toughened Poly(methyl methacrylate)

V. NELLIAPPAN,[1,2] M. S. EL-AASSER,[1,3,*] A. KLEIN,[1,3] E. S. DANIELS,[1] J. E. ROBERTS,[2] R. A. PEARSON[4]

[1] Emulsion Polymers Institute, Lehigh University, Bethlehem, Pennsylvania 18105

[2] Department of Chemistry, Lehigh University, Bethlehem, Pennsylvania 18105

[3] Department of Chemical Engineering, Lehigh University, Bethlehem, Pennsylvania 18105

[4] Department of Materials Science and Engineering, Lehigh University, Bethlehem, Pennsylvania 18105

Received 8 November 1996; accepted 10 December 1996

ABSTRACT: Two- and three-layer composite latex particles were used to prepare rubber-toughened poly(methyl methacrylate) (RT-PMMA). The interfacial thicknesses of the multilayered particles were varied by using different emulsion polymerization synthesis techniques. The resulting interphases were previously characterized by ^{13}C nuclear magnetic resonance techniques. The poly(divinyl benzene)/poly(butyl acrylate) (PDVB/PBA) interphase thickness was found to be in the range of 5–7 nm. It was also found that the PBA/PMMA interphase thickness could be varied from 5 to 7 nm (batch addition of MMA) to 15 to 17 nm (interphase compatibilized with PMMA macromonomer). The interphase thickness was expected to play an important role in the mechanical behavior of PMMA. The effect of the interphase of two- and three-layer particles on the tensile and fracture behavior of PMMA composites was evaluated. The fracture surfaces were examined by scanning electron microscopy. The two-layer PBA/PMMA particles with a thicker interphase (15–17 nm) exhibited higher K_{IC} values with the PMMA composites compared with PBA/PMMA particles with a thinner interphase (5–7 nm). The three-layer particles were found to be more effective in toughening PMMA compared with the two-layer particles. The differences in toughening behavior are speculated to arise from the morphological effects caused by a thicker interphase, which in turn results in better coverage by the PMMA shell and a more uniform distribution of the toughening particles in the PMMA matrix. © 1997 John Wiley & Sons, Inc. J Appl Polym Sci **65:** 581–593, 1997

Key words: core/shell latex; rubber-toughened PMMA; latex; mechanical behavior; fracture

INTRODUCTION

The toughness of thermoplastics such as poly(methyl methacrylate) (PMMA) and polystyrene (PS) can be improved by the addition of a rubbery phase, often without the deterioration of other desirable properties.[1] The main energy dissipative processes in rubber-toughened thermoplastics are massive matrix crazing, cavitation, and multiple localized shear bands initiated by the particles.[1] These phenomena are known to be affected by the nature of the rubber-matrix interphase and by the morphology of the rubber particles. Interphase

* *Correspondence to:* M. S. El-Aasser.

characteristics including the concentration gradient of the polymer phases, interphase thickness, thermal stability, chemical bonding, and molecular interdiffusion and interactions determine the behavior of the interphase. These characteristics of the interphase region influence the adhesion of the rubber particles to the matrix. The interphase thickness and composition can be tailored. The interphase strength between the particles and the matrix can be improved by the introduction of polymeric compatibilizers[2,3] or grafting sites, both of which result in better interfacial bonding and a well-dispersed morphology.[4]

The morphology of the toughening particles also has a large influence on the physical and mechanical behavior of the resulting toughened matrix.[5] Many of the emulsion polymerization process parameters which are varied to prepare the toughened particles have an influence on the particle morphology[6]; desired morphologies can be achieved by varying the interfacial tension, the degree of crosslinking, the mode of monomer addition, etc.[7,8] Haward and Mann investigated the effect of grafting at the acrylonitrile-butadiene-styrene (ABS) interphase and demonstrated that the techniques which produce ABS polymers with less grafting and low particle/matrix adhesion at the interphase lead to materials with inferior impact strength.[9] Bucknall et al. have attributed the impact properties of the ABS to the craze-forming ability of the rubber domains.[10]

High-impact PS (HIPS) is prepared by techniques which lead to grafting at the interphases.[1,9] Some of the early HIPS materials, which were made by melt-blending, led to less tough materials than HIPS in which the rubber was bonded to the matrix via grafting.[1] Donald and Kramer[11] studied the role of rubber particles in HIPS using transmission electron microscopy (TEM) and demonstrated that the rubber particles initiate crazes; they also act as craze terminators, preventing the growth of very large crazes. The poorly terminated crazes lead to the initiation of cracks. Aggarwal and Livigni[12] used block copolymers to increase the level of adhesion between the phases to synthesize HIPS with high-impact properties. Brown, Kramer, and colleagues[13,14] have demonstrated the applicability of small-angle X-ray scattering to study the formation of crazes in ABS and HIPS. Abate and Heikens[15] found that higher adhesive strength between glass spheres and PS increased the formation of crazes.

Chen and Jan[16] have studied the influence of the rubber-matrix interphase on the fracture behavior of epoxy resins; they modified the ductility of the interphase zone and found that the interfacial zone has a strong influence on the fracture behavior of epoxy resins by affecting the degree of cavitation. Pearson et al.[17,18] have studied the effect of the interphase on the fracture toughness of epoxy and found that the rubber-matrix interphase indirectly influences toughness by affecting the blend morphology. On the other hand, Maltonis has used numerical methods to model an isolated particle to study the effect of the interphase on the overall properties of a composite; he found that the presence of an interphase does not affect the stress fields in a composite.[19] Lu et al. have investigated the effect of the reactive coupling of the core/shell impact modifiers with nylon 6 and found that this led to tough blends.[20]

Particles in the 250-nm size range were found to be the optimal size for toughening PMMA.[21–23] PMMA can shear yield or craze depending on the testing conditions. Wrotecki et al.[22,23] also found that a certain degree of grafting at the interphase led to increased toughness. PMMA homopolymer crazing is a dominant mode of fracture.[24] Bucknall et al.[25,26] found that the inclusion of rigid phases inside the rubbery particles increased their effectiveness. Shah[27] examined the morphological features of fracture surfaces of notched Izod bars of rubber-modified PMMA and found that up to 10 wt % modifier caused PMMA to craze; at higher modifier concentrations, regions of plastic deformation as well as craze propagation regions were observed. At higher particle concentration, the features on the fracture surface were attributed to shear yielding. Frank and Lehmann[28] found that low strain rates produced shear yielding; with increasing strain rates, the contribution from the cavitation process increased, while the contribution from the shear process decreased. Lovell et al.[29,30] had studied the toughening behavior of multilayered particles consisting of radially alternating glassy and rubbery layers; the rubbery layers consisted of butyl acrylate and styrene copolymer (78.2 : 21.8 mol %), while the glassy layer consisted of methyl methacrylate and ethyl acrylate (94.9 : 5.1 mol %). They examined the effect of particle morphology and rubber phase volume fraction on the tensile and fracture properties of PMMA toughened by two-, three-, and four-layer particles and found that the three- and four-layer particles were more effective in toughening the brittle PMMA matrix. The toughening

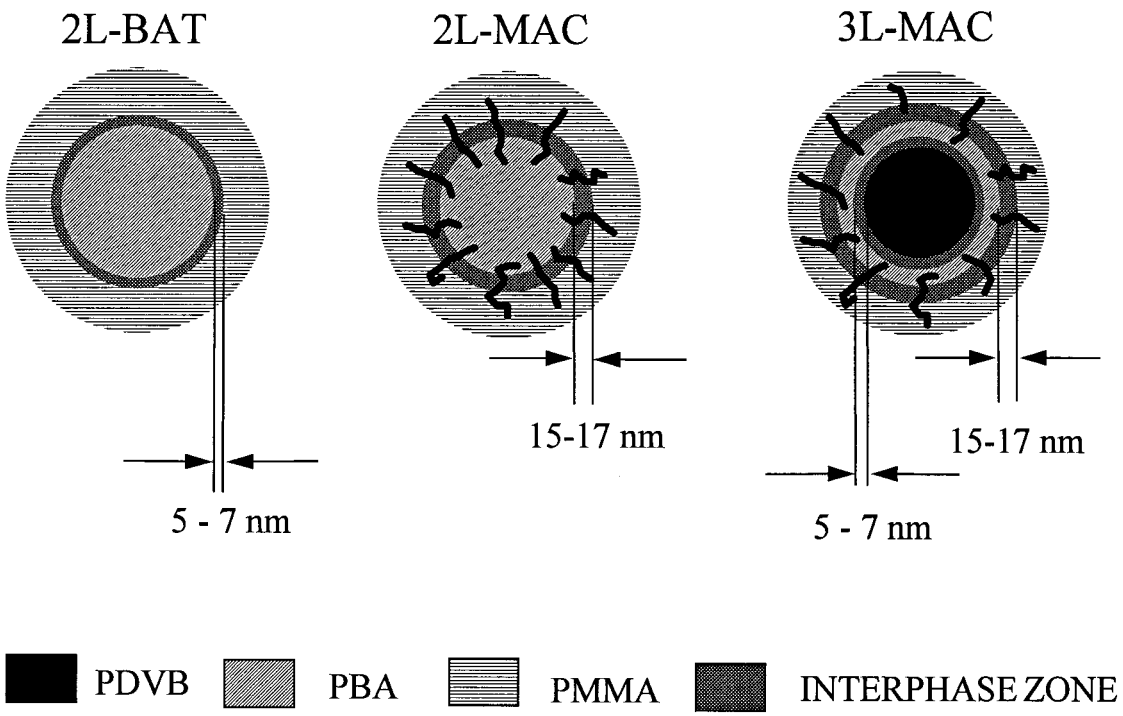

Figure 1 Schematic representation of the two-layer and three-layer particles incorporated into the PMMA matrix: (a) 2L-BAT, (b) 2L-MAC, and (c) 3L-MAC. The notation is explained in the text.

particles were found to cavitate and generate very small yield zones which run between particles roughly parallel to the crack.[31]

The current research emphasizes the effect of the interphase on the mechanical properties of PMMA composites. PMMA composites are prepared with two- and three-layer toughening particles. Different synthesis techniques were used to prepare multilayered particles with different interfacial characteristics; these were characterized by ^{13}C nuclear magnetic resonance (NMR) techniques.[32,33] This article examines the effect of the core/shell latex interphase of two- and three-layer particles on the toughening behavior of PMMA. A series of three different two- and three-layer core/shell-type latex particles with tailored interphases were used for this study; these particles are shown schematically in Figure 1. The two-layer poly(butyl acrylate) (PBA)/PMMA particles include those prepared via a batch process with an interfacial thickness of 5–7 nm (i.e., 2L-BAT) and also those particles prepared in the presence of a PMMA-macromonomer compatibilizer at the PBA/PMMA core/shell interphase (i.e., 2L-MAC), which resulted in the formation of an interphase which was more diffuse (i.e., thickness in the range of 15–17 nm).[34] The three-layer particles (i.e., 3L-MAC) have a rigid core of poly(divinyl benzene) (PDVB) with a PBA shell and an outer PMMA shell (PDVB/PBA/PMMA).

EXPERIMENTAL

Synthesis of Multilayer Composite Latexes

The PDVB/PBA core/shell latex was synthesized according to the procedures described previously.[35] The recipe and the experimental procedure used for incorporating the PMMA-macromonomer in PBA are described in greater detail by Rajatapiti et al.[2,3] The PMMA-macromonomer used was provided by E. I. Du Pont de Nemours, Inc.; its molecular weight was 4,200 g/mol. MMA was added via a semicontinuous mode of addition to the PBA seed (with PMMA-macromonomer incorporated) at a feed rate of 1.2 mL/h with a syringe pump (i.e., monomer-starved conditions) to form the shell polymer. The presence of PMMA-macromonomer grafts in the PBA phase increases the compatibility between the respective PBA/PMMA interphases.[34,35]

Table I Recipe Used for the Incorporation of PMMA-Macromonomer into the PDVB/PBA Core/Shell Latex Particles at 70°C

Components	Amount (g) (Seed Latex)	Amount (g) (Preemulsified Feed)
Aerosol AY 65[a]	0.67 [7 mM][b]	0.5 [5 mM][b]
Triton X-405[c]	1.0 [3 mM][b]	0.5 [1.5 mM][b]
BA	—	13.0
PMMA-macromonomer	—	2.0[d]
Distilled-deionized water	10	30.0
Ethanol	25	12.5
PDVB/PBA seed latex (core/shell ratio = 1 : 0.5, 20% solids)[e]	150.0	—
KPS	0.11 [2 mM][b]	

[a] Sodium diamyl sulfosuccinate (Cytec Industries).
[b] Based on the total water content.
[c] Octylphenoxy polyethoxy ethanol, molecular weight = 1,740 g/mol; manufactured by Union Carbide.
[d] 9 wt % based on the PBA phase.
[e] D_w = 192 nm and D_n = 168 nm, where D_w = weight average particle diameter and D_n = number average particle diameter.

This section will give a brief description of the synthesis of the other core/shell latexes used in this study. The poor water solubility of the PMMA-macromonomer prevents the use of conventional emulsion polymerization techniques for incorporating the macromonomer into the PBA phase of the PDVB/PBA core/shell latex. Wang[36] measured the solubility of PBA in ethanol/water mixtures and found that PBA was insoluble in cases where the weight percent of ethanol was less than 30%. An ethanol/water mixture reportedly is a good solvent for PMMA, while it is a nonsolvent for PBA.[37] The presence of ethanol in the medium was exploited to incorporate the PMMA-macromonomer into the PBA phase in the PDVB/PBA core/shell latex particles. The recipe used for the incorporation of the PMMA-macromonomer is listed in Table I. The total solids content was maintained at 20%.

The incorporation of PMMA-macromonomer into the PDVB/PBA core/shell latexes involves a four step procedure.

1. The PMMA-macromonomer was dissolved in butyl acrylate monomer in the presence of ethanol (12.5 g), followed by the addition of Triton X-405 (0.5 g) and Aerosol AY 65 (0.5 g) at 70°C. The ingredients were stirred for 1 h and then subjected to sonication with a Branson sonifier (model W-350) for 60 sec at a power level of 7.
2. After the mixture became homogenous, water was gradually added with stirring. The stirring was continued for 30 min, followed by sonification of the mixture.
3. To the seed PDVB/PBA latex was added Aerosol AY 65 (0.67 g), water, and Triton X-405 (1.0 g), which was then stirred for 30 min. This was followed by the gradual addition of ethanol (25 g) with a pipette over a 10-min period.
4. The preemulsified feed was added to the seed latex and allowed to swell the latex for 24 h at 45°C in 12-oz bottles which were tumbled end-over-end in a thermostated water bath. The polymerization was then carried out to complete conversion by injecting aqueous KPS initiator solution and heating at 70°C for 24 h. No coagulum was found. The residual ethanol in the resulting latex was extracted by azeotropic distillation. The resulting PDVB/PBA latex with PMMA-macromonomer incorporated was used as a seed in a third stage polymerization. The recipe used for the third-stage seeded polymerization (i.e., the incorporation of the PMMA shell) is given in Table II. The third-stage MMA monomer was added via a semicontinuous process under monomer-starved conditions at an addition rate of 2 mL/h. The particle size and size distributions were obtained by

Table II Recipe Used for the Third-Stage Polymerization of MMA (PMMA Shell) into the PDVB/PBA Core/Shell Latex Particles at 70°C

Components	Amount (g) (Seed Latex)
PDVB/PBA seed latex (1 : 1) (20% solids)[a]	100.0
MMA	20.0
Distilled-deionized water	80.0
Aerosol AY 65	0.1 [10 mM][b]
KPS	0.1 [2 mM][b]
Percent solids	20%

[a] D_w = 214 nm and D_n = 189 nm.
[b] Based on the total water content.

TEM. The particle size results are listed in Table III. Over 500 particles were counted for the determination of each particle diameter. The PBA/PMMA core/shell latex compatibilized with PMMA-macromonomer (2L-MAC) has the highest polydispersity index (PDI; equal to D_w/D_n). This is because of the initial broad distribution of the PBA-g-PMMA-macromonomer, which was prepared via a miniemulsion technique. However, as a third layer of PMMA is added, the PDI narrows down to about 1.13 because of the competitive growth effect (i.e., 3L-MAC).

PMMA homopolymer latex was prepared by mixing MMA monomer with aqueous surfactant solution for 1 h with a magnetic stirrer, followed by homogenization for 1 min with a sonifier, and then polymerization at 70°C for 12 h. The recipe used is identical to the recipe used for the preparation of PBA seed latex, shown in Table IV. For this purpose, MMA monomer was substituted for BA monomer.

The PBA/PMMA core/shell latexes were prepared according to the recipe given in Table IV. First, the seed PBA latex was synthesized according to the recipe listed in Table IV. The surfactant used was Aerosol AY 65 (Cytec Industries; sodium diamyl sulfosuccinate). For the second-stage seeded batch polymerization, the potassium persulfate (KPS) initiator was added after swelling of the PBA seed with MMA monomer overnight; the batch polymerization was carried out in a bottle poymerizer by tumbling end-over-end at 70°C for 24 h. The polymer-to-monomer ratio was 1 : 1. The number (D_n) and weight average (D_w) particle sizes were analyzed by Capillary Hydrodynamic Fractionation (Matec, Model 1100); the results are given in Table III.

Characterization of the Structured Latexes Using Electron Microscopy

The morphologies of the resulting latexes were observed with a Phillips 400 transmission electron microscope. The latexes were stained with uranyl acetate (negative stain) and/or ruthenium tetroxide, which stains the PBA phase (positive stain). Diluted latex samples were cast on stainless-steel transmission electron microscope grids, were repeatedly exposed to vapors of ruthenium tetroxide to ensure adequate contrast between the PBA and PMMA phases, and were imaged with a cold-stage attachment. Figure 2(a) depicts the PBA/PMMA core/shell latexes prepared via a batch process without the incorporation of PMMA, while Figure 2(b) shows the PBA/PMMA core/shell particles prepared with PMMA-macromonomer compatibilizer. The PBA phase appears dark, and the PMMA domains appear light. Fig-

Table III The Different Types of Toughening Particles Incorporated into a PMMA Matrix

Toughening Particles	Notation	D_n (nm)	D_w (nm)	D_w/D_n
PBA/PMMA core/shell latex; MMA added via a batch process (two-layer particles)	2L-BAT	254	267	1.05
PBA/PMMA core/shell latex; compatibilized with PMMA-macromonomer; MMA added semicontinuously (two-layer particles)	2L-MAC	228	274	1.20
PDVB/PBA/PMMA three layer latex; BA added to PDVB; PBA/PMMA compatibilized with PMMA-macromonomer (three-layer particles)	3L-MAC	231	261	1.13

Table IV Recipe Used for the Preparation of PBA Seed Latex via Emulsion Polymerization and PBA/PMMA Core/Shell Latex Particles via Seeded Emulsion Polymerization at 70°C

Components	Amount (g) (Seed Latex)	Amount (g) (Second Stage)
BA[a]	40	0
MMA	0	40
Distilled-deionized water	160	160
Aerosol AY 65[b]	0.6646	0
KPS	0.2	0.2
Percent solids	20%	20%

[a] PBA seed latex prepared with and without PMMA-macromonomer.
[b] Sodium diamyl sulfosuccinate (Cytec Industries).

ure 3(a) shows the PDVB seed latex stained with phosphotungstic acid only; microgels are not detected. Figure 3(b–d) are stained lightly with positive and negative stains; the dark phase in Figure 3(b and c) is the PDVB phase, while the lighter phase is the PBA phase. As expected, there is a greater volume of PBA phase in Figure 3(c); also, no secondary particles are detectable. Figure 3(d) is the micrograph of the three-layer particles stained with both positive and negative stains. The dark cores may result from the stained PDVB and PBA phases. The sizes of the particles appear to be larger, and the size distribution appears to be narrower, than the two-layer particles.

Variation and Characterization of the Interphase Zone

The relatively small volume of the interphase makes it difficult to study in the presence of bulk polymer. Nzudie et al. had previously used $[H]T_1\rho$ relaxation measurements to characterize the interphase of polybutadiene/PMMA core/shell latexes.[32,33] Emphasis was placed on the synthesis and characterization of core/shell latex particle interphases. The copolymerization of PMMA-macromonomer with *n*-butyl acrylate, followed by the addition of a PMMA shell layer, enhanced the interfacial thickness.[34] Nelliappan et al.[34,35] have previously applied similar solid-state ^{13}C NMR techniques to characterize the PDVB/PBA interphase[34] and to study the effect of

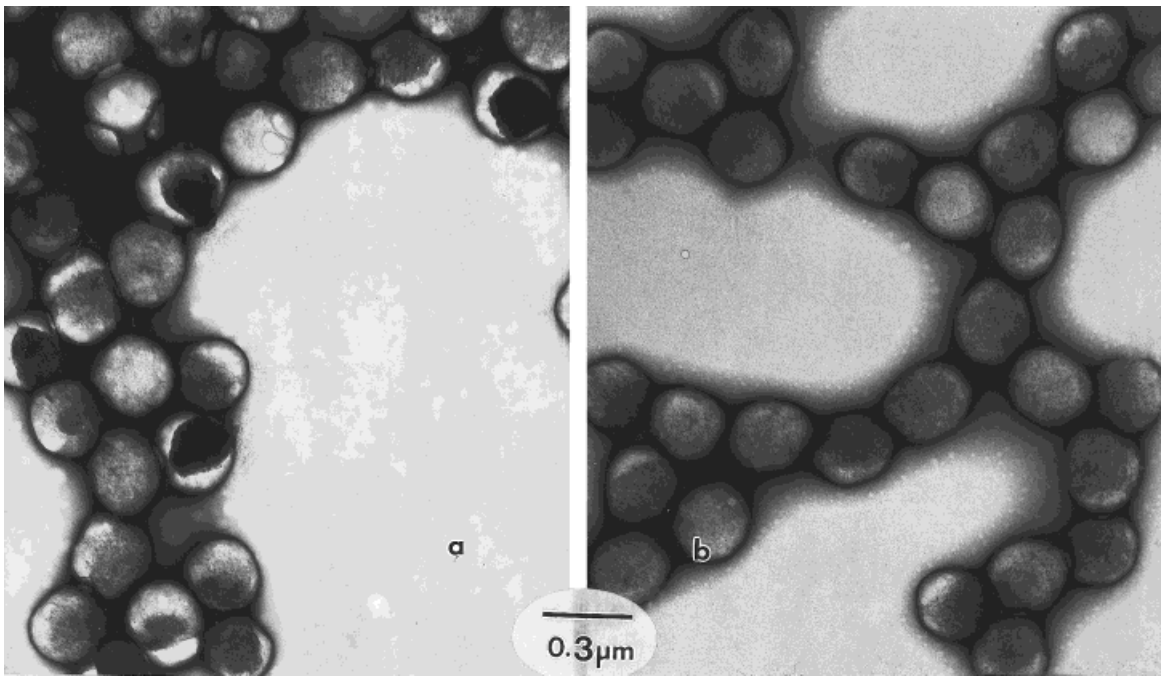

Figure 2 Transmission electron micrographs showing: (a) the PBA/PMMA core/shell latex prepared via batch process (no macromonomer) and (b) the PBA/PMMA core/shell latex with macromonomer incorporated. Samples were stained with uranyl acetate and/or RuO_4. The PBA phase appears dark, and the PMMA phase is light.

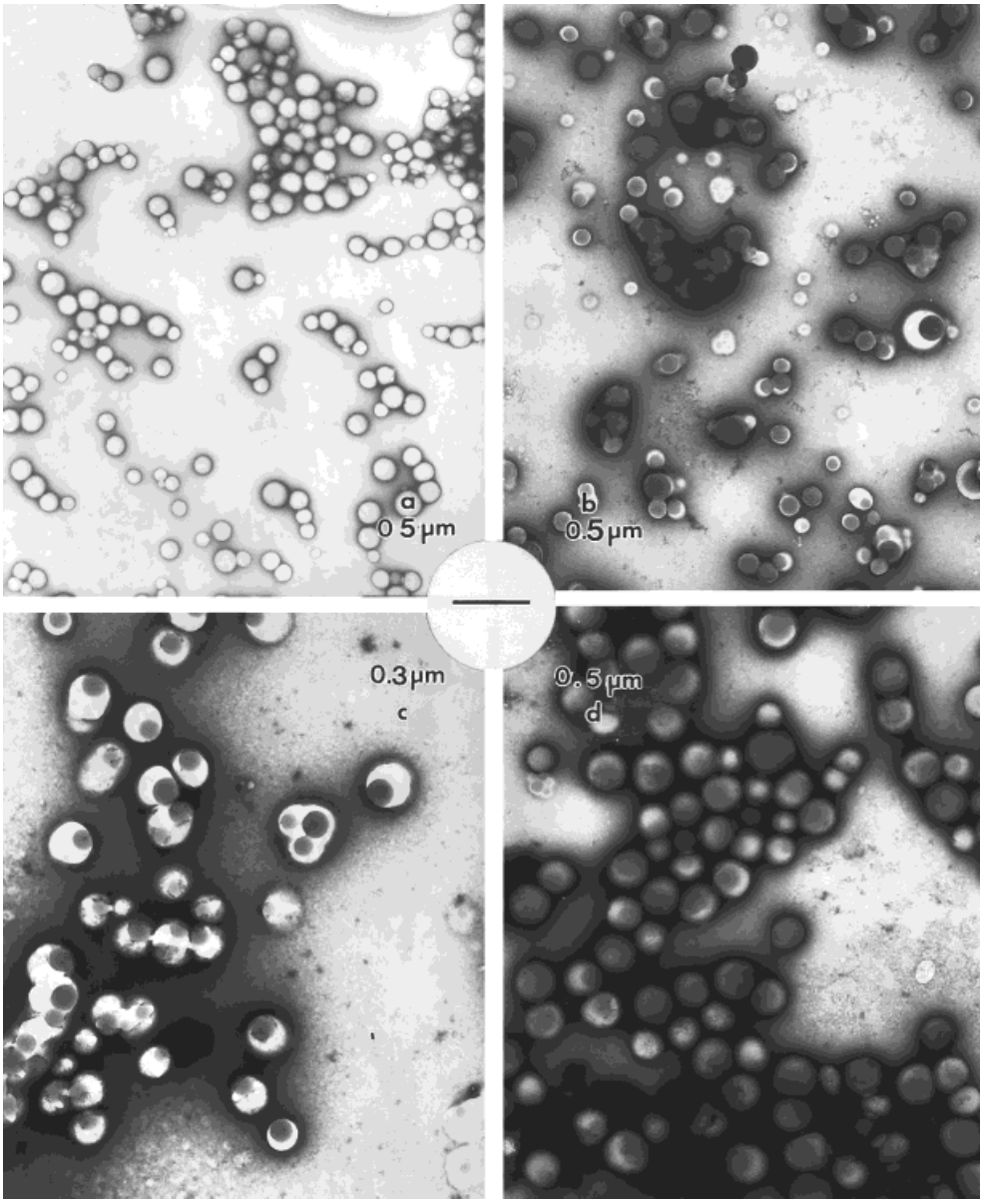

Figure 3 Transmission electron micrographs showing: (a) PDVB seed, (b) PDVB/PBA core/shell latex, (c) PDVB/PBA core/shell latex with macromonomer incorporated, and (d) PDVB/PBA/PMMA core/shell/shell-type particles. Phosphotungstic acid is used as a negative stain in all cases, and ruthenium tetroxide is used as a positive stain in panels b, c, and d. The PDVB phase appears dark, and PMMA and PBA are lightly stained in panels b, c, and d.

PMMA compatibilizer on the PBA/PMMA core/shell latex particle interphase.[35] PBA/PMMA core/shell latex particles could be prepared with differing interphase thicknesses, depending on the process conditions. The use of a PMMA-macromonomer compatibilizer increased the thickness of the PBA/PMMA core/shell latex interphase from 10 to 11 nm to 15 to 17 nm. On the other hand, the PBA/PMMA core/shell particles prepared via the addition of MMA in a batch process resulted in the formation of interphase zones with thicknesses in the range of 5–7 nm. The interphase thickness for PDVB/PBA core/shell latexes was in the range of 5–7 nm, and the thickness was not influenced by aging. The presence of residual double bonds at the PDVB/PBA in-

terphase possibly led to the interphase being kinetically "frozen-in."

Preparation of Toughened PMMA Blends

A list of the toughening particles, the notation used, and their size distributions are given in Table III. A PMMA homopolymer latex was synthesized according to the recipe listed in the first column of Table IV, adding the same weight of MMA instead of BA monomer. This resulted in the formation of latexes of particle size D_n = 280 nm and D_w = 295 nm. This PMMA homopolymer latex was blended with the multilayer composite latex particles in an 80/20 wt % ratio of PMMA-latex/toughening particles. An 80/20 blend of PMMA latex and PBA/PMMA core/shell latex compatibilized with PMMA-macromonomer is denoted as PMMA/2L-MAC. This resulted in an overall rubber volume fraction of 10%.

The latexes were stirred in a beaker with a magnetic stirrer for 12 h at room temperature and then dried. Residual water was removed by drying the blended latex at room temperature, followed by grinding the resultant polymer into a fine powder. Methanol was added to the resulting powder to remove residual surfactant, initiator, etc.; the mixture was then sonified for 30 sec to break up the flocs. The methanol was then removed by vacuum filtration with a fritted glass filter and a Buchner funnel. This was followed by washing with hot water and drying the resultant mixture in a vacuum oven for 24 h at 40°C. This process resulted in the purification of the polymer powders.

Determination of Mechanical Behavior

The purified polymer powders were then compression molded at 5,000 psi at 135°C for 20 min into bars of 6 × 1 × 0.2 cm with a Carver hot press. The resulting compression-molded samples were machined into ASTM D 638 Type V standard tensile specimens with a Dremel moto-tool and then polished. The gauge length (the narrow region of the dog bone–shaped specimens) had a width of 2.5 mm. The tensile strength was measured by use of the ASTM D 638 test method with a crosshead speed of 10 mm/min; five specimens were used for each test. The tensile results for specimens which failed in the grips were discarded. The dispersability of the composite latex particles in the PMMA matrix was studied by observing the fracture surfaces with a scanning electron microscope (SEM) (JEOL 6300). The surfaces were coated with a 0.5-mm gold/palladium alloy and examined at a magnification of 10,000×.

ASTM D 5045-91 single-edge-notched three-point-bend geometry (SEN-3PB) specimens were also prepared via compression molding under the same conditions, and a crack was initiated at the notch with a fresh razor blade. The critical stress intensity factor, K_{IC}, was determined by use of an ASTM D5045-91 test method with a SEN-3PB specimen with dimensions of 6.4 × 12.7 × 80 mm. The tests were performed on an Instron 1011 machine with a 100-lb load cell at a crosshead speed of 1 mm/min. Five specimens were used for the determination of each K_{IC} value. The K_{IC} was calculated from the following equation:

$$K_{IC} = Y \frac{3PSa^{1/2}}{2tw^2} \quad (1)$$

where P is the critical load for crack propogation, S is the span length, a is the crack length, t is the thickness, w is the width, and Y is a nondimensional shape factor given by

$$Y = 1.9 - 3.07\,(a/w) + 14.53\,(a/w)^2 - 25.11\,(a/w)^3 + 25.8\,(a/w)^4 \quad (2)$$

The thickness, t, was maintained so as to provide a plane strain constraint; the span, S, was set to four times the specimen width:

$$t > 2.5\,(K_{IC}/\sigma_y) \quad (3)$$

The dynamic mechanical properties of the PMMA/toughening particle composites were measured to obtain storage modulus (G''), loss modulus (G''), and tan δ (G''/G'). Compression-molded samples with dimensions of 40 × 10 × 1 mm were used as specimens. The viscoelastic properties were measured with a Rheometric Dynamic Analyzer (RDA II). A frequency of 1 rad/sec was used over the temperature range of 30–180°C.

Examination of the Fracture Surfaces

The degree of dispersibility of the multilayered particles in the PMMA matrix was examined by scanning electron microscopy of the fracture surfaces of the SEN-3PD specimens. The fracture

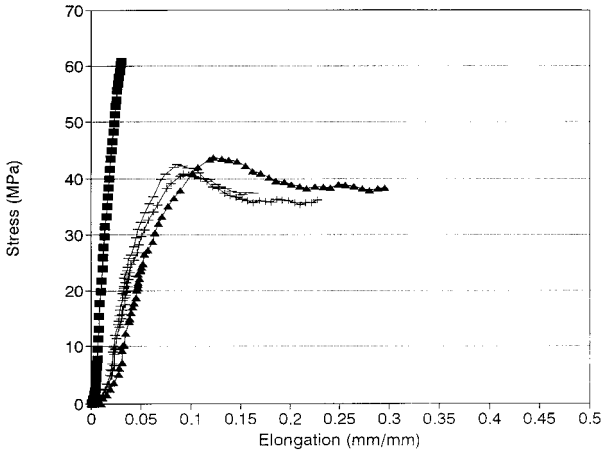

Figure 4 Stress versus strain plots of (■) PMMA homopolymer and PMMA blended with two-layer particles: (−) PMMA/2L-BAT, (+) PMMA/2L-MAC, and (▲) PMMA/3L-MAC particles.

surfaces were coated with a 0.5-nm-thick gold/palladium layer to dissipate charge buildup on the surface of the specimens.

RESULTS AND DISCUSSION

Mechanical Behavior of the Blends

Tensile Strengths

The stress-strain plots of PMMA composites prepared with the two types of two-layer and the three-layer latex particles are compared with PMMA homopolymer in Figure 4. The particles incorporated into the PMMA matrix were PBA/PMMA core/shell latex with MMA added via a batch mode (2L-BAT) and PBA/PMMA particles compatibilized with PMMA-macromonomers (2L-MAC). The yield stress and the moduli are listed in Table V. The PMMA homopolymer was found to undergo a brittle fracture at ~ 2.5%; a PMMA matrix exhibits a brittle type of failure by a breakdown of crazes.[38] As can be seen in Figure 4, the PMMA/2L-BAT composite undergoes less extension (~ 15%) compared with the PMMA/2L-MAC (~ 23%). Also, the yield stress is slightly lower for the PMMA/2L-MAC composites. In the two-layer series, the Young's modulus value is lowest for the PMMA/2L-MAC composite. At the onset of yielding, stress-whitened regions appeared and increased in intensity until fracture occurred. The two-layer particles incorporated in the PMMA composites probably undergo cavitation and debonding; this leads to the stress whitening observed in the tensile tests.

As mentioned before, the PBA/PMMA particles prepared by a batch method have a thinner interphase zone (5–7 nm) compared with the PBA/PMMA particles with a compatibilized interphase (15–17 nm).[35] The thinner interphase results from a lower amount of interdiffusion and grafting between the two phases, while the compatibilized interphase exhibits more ductility and molecular interdiffusion, resulting in better adhesion. The energy required to fracture the interphase is a result of three molecular mechanisms: chain stretching, chain scission, and chain pullout. The pullout and scission are expected to be dominant in this case because the molecular weight of the PMMA is below the critical entanglement molecular weight of 28,000 g/mol.[39,40] Grafting of PMMA to the PBA would result in internal cavitation, because the fracture energy contributions arising from chain scission and pullout would be substantially higher as the PMMA molecular weight becomes higher than the critical entanglement molecular weight.[39,40] Lovell et al.[41] observed that volume strains are negligible during the tensile strain of rubber-toughened PMMA materials and attributed shear yielding to be the

Table V Tensile Properties of PMMA Toughened with Core/Shell-Type Latex Particles

Type of PMMA/ Toughening Particle Composites	Tensile Yield Stress (σ_Y) (MPa)	Young's Modulus (E) (GPa)	Extension (%)
PMMA/2L-BAT	42.5 ± 2.0	1.89 ± 0.20	15 ± 3
PMMA/2L-MAC	40.8 ± 2.0	1.75 ± 0.20	23 ± 4
PMMA/3L-MAC	43.8 ± 2.0	1.61 ± 0.20	30 ± 6
PMMA homopolymer	61.0 ± 2.0[a]	3.10 ± 0.20	2.0 ± 0.40

[a] Fracture stress.

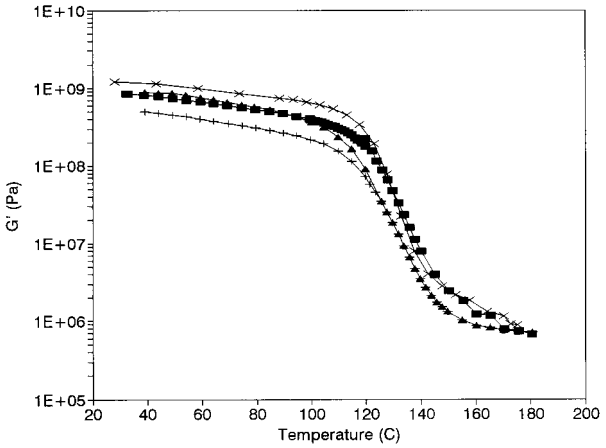

Figure 5 Temperature dependence of storage modulus (G′) for (×) PMMA, (■) PMMA/3L-MAC, (+) PMMA/2L-MAC, and (▲) PMMA/2L-BAT.

major mechanism of toughening at low strain rates. The short-chain macromonomer probably alters the morphology of the core/shell particles, resulting in higher extensions for the 2L-MAC and 3L-MAC composites. If the rubber particles are well bonded to the matrix, the particles act as stress concentrators, and because of the volume constraint, this leads to a state of triaxial stress. It is this triaxial stress which promotes deformation processes.

Figure 4 also compares the stress-strain plots of the PMMA homopolymer with the PMMA toughened with three-layer particles. These composites are denoted as PMMA/3L-MAC. The Young's modulus of the PMMA/2L-MAC composite is slightly greater than the PMMA/3L-MAC composites; the yield stress is higher for the PMMA/3L-MAC composites compared with the PMMA/2L composites. However, the extension of the PMMA/3L-MAC composite is $\sim$ 30%, which is significantly higher than that of the two-layer series, for which the extension is in the range of 15–23%. Guild et al.[42] have used finite element analysis to compare the stresses in the rubbery phase in two- and three-layered particles. Their calculations reveal that the hydrostatic stress in the rubbery annulus of a three-layered particle is greater than that in the rubber phase in two-layered particle, while the direct stress concentration is greater for a two-layer particle.

Dynamic Mechanical Analysis

Figure 5 displays the temperature dependence of the storage modulus (G') for the PMMA homopolymer and also for the PMMA composites prepared with the core/shell particles. The G' of all of the samples drops rapidly to about 10^6 Pa at around 120°C. However, between 30 and 100°C, the PMMA homopolymer has the highest values of G', followed by both the PMMA/3L-MAC and the PMMA/2L-BAT composites. The PMMA/2L-MAC composites exhibited the lowest values of G'. The PMMA/2L-MAC has an interphase zone with a thickness in the range of 15–17 nm; this could possibly result in a higher rubber volume fraction because of the increased contribution from the interphase. The contribution to the interfacial PMMA in the case of PMMA/2L-BAT composites is expected to be much less because the interphase thickness is in the range of 5–7 nm. This leaves the PMMA matrix less perturbed, and the values of G' are expected to be closer to that of the PMMA homopolymer.

The G'-temperature curves for the PMMA/3L-MAC composites almost overlap with the G'-temperature profile of the PMMA/2L-BAT. However, in the former case, even though the weight fraction of the modifier is the same as in the other cases (20%), the weight fraction of the rubber phase is 10%, because the PDVB core accounts for the remaining 10%. This probably offsets the contribution from a thicker interphase. The following section examines the fracture toughness of the various composites.

Fracture Characterization

The K_{IC} values are summarized in Table VI. The two-layer particles increased the base K_{IC} values of the PMMA homopolymer by a factor of 2 to about 2.3–2.6 MPa $m^{1/2}$, while the three-layer particles increased the K_{IC} values to about 2.8 MPa $m^{1/2}$. Thus, the inclusion of the two-layer and three-layer particles resulted in an increase in the toughness values compared with the homopolymer. The 2L-MAC and 3L-MAC particles imparted higher values of fracture toughness to the PMMA matrix compared with the 2L-BAT particles. These values of K_{IC} compare well with the maximum values of K_{IC} reported by Lovell et al.[41] for two-layer and three-layer particles, which are in the range of 2.8 MPa $m^{1/2}$.

As mentioned before, this is a result of the thicker interphases present in 2L-MAC and 3L-MAC (see Table VI); a thicker interphase results in more interdiffusion of the PBA and PMMA phases and entanglement of the PMMA-macro-

Table VI Summary of K_{IC} and Interphase Thickness Values of the PMMA-Based Composites

Sample Description	K_{IC} (MPa $m^{1/2}$)[a]	Interphase Thickness (nm)
PMMA homopolymer	1.30 ± 0.06	—
2L-BAT/PMMA	2.30 ± 0.06	5–7[34]
2L-MAC/PMMA	2.60 ± 0.06	15–17[35]
3L-MAC/PMMA	2.80 ± 0.06	5–7[34] (PDVB/PBA interphase), 15–17 (PBA/PMMA interphase[35])

[a] An average of five measurements per sample.

monomer, resulting in increased rubber fraction and increased adhesion. A more uniform morphology was also found to result from the inclusion of PMMA-macromonomer.[35] A combination of one or more of the above-mentioned parameters, such as morphology and rubber fraction, results in higher K_{IC} values for the 2L-MAC and 3L-MAC cases.

Lovell et al. had also studied the effect of the volume fraction of the rubbery inclusions on the fracture toughness (K_{IC}) of the composites. The deformation micromechanics of SEN-3PB samples of rubber-toughened PMMA was studied by the use of TEM; the presence of microcrazes was detected.[41] As mentioned before, Guild et al.[42] used finite element analysis to investigate the effect of a rigid subinclusion inside a rubbery particle on the toughening behavior; they had found that the rigid subinclusion (i.e., a three-layer particle) affected the hydrostatic tension in the rubber annulus. In this case, the highly crosslinked PDVB core was chosen as the glassy core because it has residual double bonds on the surface which can graft with PBA. The fracture surfaces of the SEN-3PB specimens were examined with an SEM.

Examination of the Fracture Surfaces: Scanning Electron Microscopy

It may be noted in the scanning electron micrographs shown in Figure 6(a–d) that there are significant differences in the roughness of the fracture surfaces of PMMA homopolymer and PMMA, which was toughened with the multilayer composite particles. PMMA homopolymer typically fractures by the breakdown of crazes along its center, which leaves a relatively smooth surface.[38] The plate-like features seen in Figure 6(a) are probably broken remnants of crazes. In the cases where the two- and three-layer particles were blended with PMMA, a very rough fracture surface was observed. These surfaces also exhibit holes, which are in the same diameter range as the toughening particles. These arise from internal cavitation and/or debonding of the toughening particles at the internal interfaces. The toughening particles do not appear to debond from the matrix in Figure 6(b–d).

CONCLUSIONS

In this investigation, the effects of the core/shell latex interphase on the mechanical behavior of PMMA composites toughened with multilayer particles were investigated. Two-layer PBA/PMMA core/shell latex particles and three-layer PDVB/PBA/PMMA particles with PMMA-macromonomers, the interphases of which were previously characterized by ^{13}C NMR relaxation techniques,[34,35] were used for this study. The PMMA-macromonomers were responsible for increasing the thickness of the interphase, which should diffuse the stress gradient at the interphases for the particles prepared with the compatibilizing agent. The PBA/PMMA core/shell particles with a thinner interphase (5–7 nm) were prepared via a batch addition of the MMA.

The tensile and fracture properties of the different blends were measured, and the fracture surface were observed with an SEM. Also, the storage modulus (G') was measured over a temperature range of 30–180°C. It was found that the interphases present in PBA/PMMA core/shell particles influenced the mechanical properties of composites prepared with PMMA. Most likely, the macromonomer facilitated complete particle coverage (see Fig. 2). This was reflected in the K_{IC}

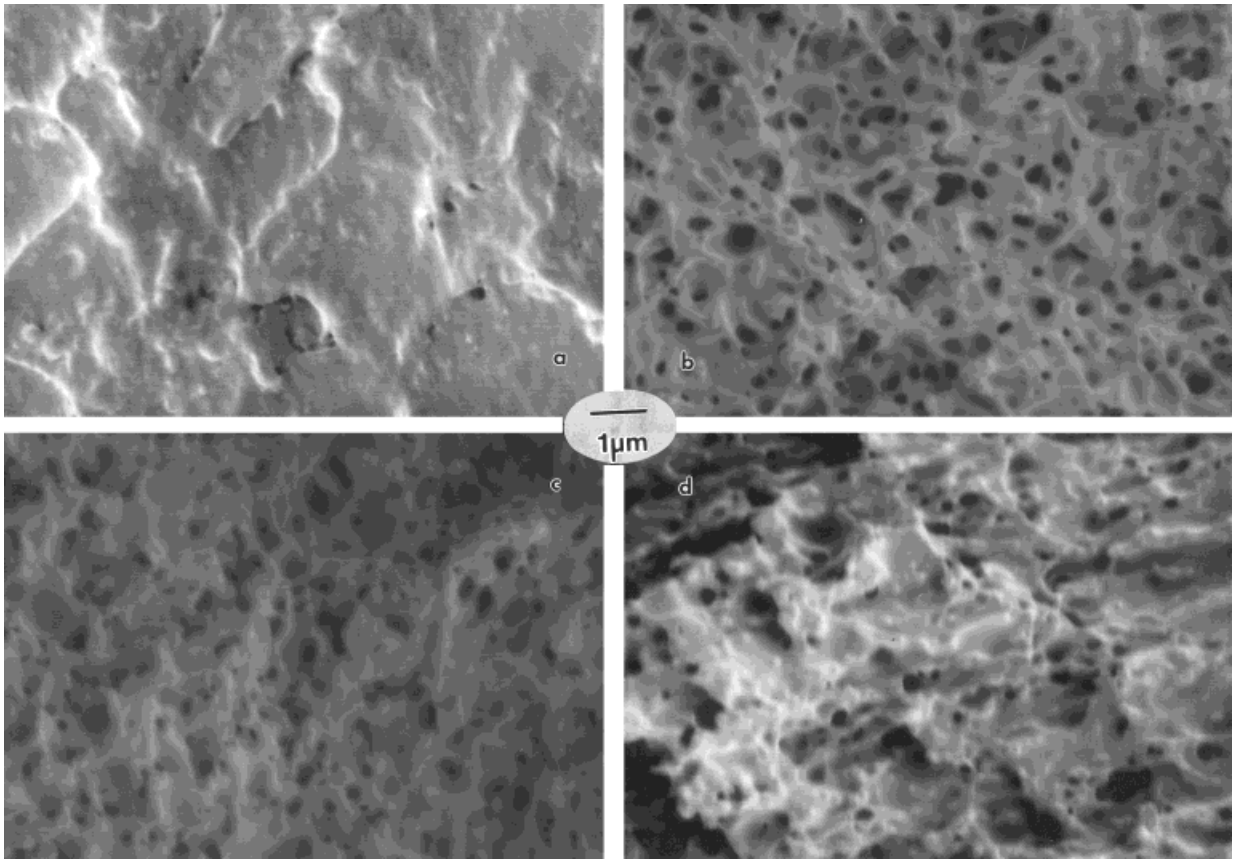

Figure 6 Scanning electron microscopy micrographs of the fracture surface of: (a) PMMA homopolymer, (b) PMMA/2L-BAT, (c) PMMA/2L-MAC, and (d) PMMA/3L-MAC. Holes are seen in panels b to d, where the toughening particles debond.

values; the K_{IC} values were higher in the PBA/PMMA blends which had a thicker interphase (PMMA/2L-MAC and PMMA/3L-MAC compared with PMMA/2L-BAT). The PMMA/3L-MAC composites, which included rigid PDVB inclusions, exhibited the highest fracture toughness values. The increased toughness values in the case of PMMA/2L-MAC and PMMA/3L-MAC are attributable to the effects of PMMA-macromonomer on the morphology by facilitating surface coverage. They also increase the rubber content by increasing the thickness of the interphase zone. The higher toughness values for the PMMA/3L-MAC blends could result from more crazes being initiated per particle, leading to multiple crazing. The K_{IC} values are lowest for the PMMA/2L-BAT composites. In this case, the segregation of 2L-BAT particles due to incomplete coverage of the rubber core (see Fig. 2) may account for the lower K_{IC} values.

The assistance of Mrs. O. L. Shaffer in scanning electron microscopy analysis is greatly appreciated.

REFERENCES

1. C. B. Bucknall, *Toughened Plastics,* Applied Science Publishers Ltd., London, 1977.
2. P. Rajatapiti, V. L. Dimone, and M. S. El-Aasser, *J. Macromol. Sci. Chem.,* **32,** 1445 (1995).
3. P. Rajatapiti, V. L. Dimone, and M. S. El-Aasser, *J. Appl. Polym. Sci.,* to appear.
4. W. J. Coumane, D. Heikens, and S. D. Sjoerdsma, *Polymer,* **21,** 103 (1980).
5. A. C. Archer, P. A. Lovell, J. McDonald, M. N. Sherrat, and R. J. Young, *Mat. Res. Soc. Symp. Proc.,* **274,** 17 (1992).
6. D. R. Stutman, A. Klein, M. S. El-Aasser, and J. W. Vanderhoff, *Ind. Chem. Prod. Res. Dev.,* **24,** 404 (1985).

7. Y. C. Chen, V. L. Dimonie, and M. S. El-Aasser, *J. Appl. Polym. Sci.,* **41,** 1425 (1990).
8. A. Rudin, *Makromol. Symp.,* **92,** 53 (1995).
9. R. N. Haward and J. Mann, *Proc. Roy. Soc.,* **A282,** 120 (1964).
10. C. B. Bucknall, C. J. Page, and V. O. Young, *Adv. Chem. Ser.,* **154,** 179 (1974).
11. A. M. Donald and E. J. Kramer, *J. Appl. Polym. Sci.,* **27,** 3729 (1982).
12. S. L. Aggarwal and R. A. Livigni, *Polym. Eng. Sci.,* **17,** 498 (1977).
13. H. R. Brown and E. J. Kramer, *J. Makromol. Sci. Phys.,* **B19**(3), 487 (1981).
14. R. A. Bubeck, D. J. Buckley, Jr., E. J. Kramer, and H. R. Brown, *J. Mater. Sci.,* **26,** 6249 (1991).
15. G. F. Abate and D. Heikens, *Polym. Commun.,* **24,** 342 (1983).
16. T. K. Chen and H. Y. Jan, *Polym. Eng. Sci.,* **31,** 577 (1991).
17. J. Y. Qian, R. A. Pearson, V. L. Dimonie, and M. S. El-Aasser, *J. Appl. Polym. Sci.,* **58,** 439 (1995).
18. R. A. Pearson and A. F. Yee, *J. Mater. Sci.,* **26,** 3844, (1991).
19. V. A. Maltonis, *Polym. Eng. Sci.,* **9,** 100 (1969).
20. M. Lu, H. Keskkula, and D. R. Paul, *Polym. Eng. Sci.,* **30,** 1373 (1990).
21. J. M. Gloaguen, P. Heim, P. Gaillard, and J. M. Lefebvre, *Polymer,* **33,** 4741 (1992).
22. C. Wrotecki, P. Heim, and P. Gaillard, *Polym. Eng. Sci.,* **31,** 213 (1991).
23. C. Wrotecki, P. Heim, and P. Gaillard, *Polym. Eng. Sci.,* **31,** 218 (1991).
24. A. J. Kinloch and R. J. Young, Eds., *Fracture Behavior of Polymers,* Applied Science Publishers, Essex, England, 1983.
25. C. B. Bucknall and R. R. Smith, *Polymer,* **6,** 437 (1965).
26. C. B. Bucknall, I. K. Partridge, and M. V. Ward, *J. Mater. Sci.,* **19,** 2064 (1984).
27. N. Shah, *J. Mater. Sci.,* **23,** 3623 (1988).
28. O. Frank and J. Lehmann, *Coll. Polym. Sci.,* **264,** 481 (1986).
29. P. A. Lovell, J. McDonald, D. E. J. Saunders, and R. J. Young, *Polymer,* **34,** 61 (1993).
30. P. A. Lovell, *Makromol. Symp.,* **92,** 71 (1995).
31. P. A. Lovell, J. McDonald, D. E. J. Saunders, M. N. Sherrat, and R. J. Young, *Mat. Res. Soc. Symp. Proc.,* **274,** 17 (1992).
32. D. T. Nzudie, L. Delmotte, and G. Riess, *Makromol. Chem. Rapid Commun.,* **12,** 251 (1991).
33. D. T. Nzudie, L. Delmotte, and G. Riess, *Makromol. Chem. Phys.,* **195,** 2723 (1994).
34. V. Nelliappan, M. S. El-Aasser, A. Klein, E. S. Daniels, and J. E. Roberts, *J. Appl. Polym. Sci.,* **58,** 323 (1995).
35. V. Nelliappan, M. S. El-Aasser, A. Klein, E. S. Daniels, and J. E. Roberts, *J. Polym. Sci., Polym. Chem.,* to appear.
36. D. Wang, *Emulsion Polymers Institute's Graduate Research Progress Report,* No. 41, 189, Lehigh University, Bethlehem, PA, 1994.
37. J. Brandrup and E. H. Immergut, Eds., *Polymer Handbook,* Wiley-Interscience, New York, 1975.
38. H. R. Brown and I. M. Ward, *Polymer,* **14,** 469 (1973).
39. M. Sambasivam, A. Klein, and L. H. Sperling, *Macromolecules,* **28,** 152 (1995).
40. L. H. Sperling, A. Klein, M. Sambasivam, and K. D. Kim, *Polym. Adv. Technol.,* **5,** 453 (1994).
41. P. A. Lovell, A. J. Ryan, M. N. Sherrat, and R. J. Young, *Polym. Mat. Sci. Eng.,* **70,** 155 (1994).
42. F. J. Guild, R. J. Young, and P. A. Lovell, *J. Mater. Sci. Lett.,* **13,** 10 (1994).